A Comparative Investigation of a New Continuous Voltage Conversion Ratio Approach in a Zero-Inductor Voltage Converter

1st Sina Salehi Dobakhshari
Department of Electrical and Computer Engineering
Queen's University
Kingston, Canada
s.salehidobakhshari@queensu.ca

2nd Aamna Nasir Hameed
Department of Electrical and Computer Engineering
Queen's University
Kingston, Canada
21anh2@queensu.ca

3rd Binghui He
Department of Electrical and Computer Engineering
Queen's University
Kingston, Canada
binghui.he@queensu.ca

4th Mojtaba Forouzesh
Department of Electrical and Computer Engineering
Queen's University
Kingston, Canada
m.forouzesh@queensu.ca

5th Yan-Fei Liu
Department of Electrical and Computer Engineering
Queen's University
Kingston, Canada
yanfei.liu@queensu.ca

***Abstract*—This paper investigates the performance of the new pulse pattern strategy for a Zero-Inductor Voltage (ZIV) converter. Unlike the other methods introduced in the literature, this method does not need additional components or sensors. Moreover, it extends the voltage conversion ratio from zero to input voltage, just like a conventional buck converter, but eliminates its drawbacks. The new method will be discussed and compared to a 3-level buck converter, and its performance as a solar battery charger will be analyzed. The results for a 250W prototype (20-60V input voltage, 12V output voltage, 21A output current) with average efficiency over the full line and load (60W to 250W) of 97.54%, are presented to justify the merit of the new method.**

***Index Terms*—Full voltage conversion range, high efficiency, switched capacitor converter, zero-inductor-voltage.**

I. Introduction

Zero-Inductor Voltage (ZIV) converters are well-known for high power density and high efficiency [1]. However, as with many other capacitive-based converters (multi-level, switched capacitor converters, etc.) the inherent fixed voltage conversion ratio has limited its application. It would be desirable to have voltage conversion flexibility as a conventional buck converter without drawbacks. Some methods are proposed in the literature to extend the voltage conversion ratio in capacitive-type converters. In [2], the voltage conversion ratio of a switched-capacitor converter (SCC) has been extended, but the proposed method uses an additional switched capacitor-inductor network for the voltage regulation, and the conversion range is, however, from zero to a maximum of 0.3. In [3], a buck converter is merged with a Resonant Switched Capacitor Converter (RSCC) to regulate the output voltage. The voltage conversion range is from zero to 1/3, which is still narrow. Another control method for an RSCC is proposed in [4]. Although it has reached very high efficiency (¿98%), the voltage conversion range is between 1/3 and 2/3. The phase shift control is introduced in [5], for a multilevel modular RSCC. Although this method does not need any extra components, the conversion range is highly limited to 0.17-0.2. One of the popular control methods in resonant switched-capacitor converters is frequency modulation.

Some RSCCs have achieved a full voltage conversion ratio through frequency control methods, as demonstrated in [6] and [7]. In [6], the RSCC attains a full voltage conversion range by using a combination of frequency and phase shift control. However, this approach requires sensing the resonant tank current, and the maximum efficiency achieved is 91%. The converter in [7] offers a wide conversion range from 0.5 to 2, allowing it to step up the input voltage. However, its maximum efficiency is 90%, which is achieved at a unity voltage ratio.

In this paper, a new control method for a ZIV converter will be discussed. The new method proposes a new gate pulse pattern strategy to fully regulate the output voltage from zero to V_{in}, without using any additional component and additional feedback signal. The converter uses seven low-voltage regular silicon switches, and the results will be compared with a Three-Level Buck Converter (TLBC) in [8] which not only uses GaN switches, but the number of switches is also less than the ZIV converter. Moreover, the converter's performance in a solar battery charger application will be investigated.

As shown in Fig. 1, the converter consists of two stages and an output filter. The first stage includes four switches (S_1, S_2, S_3, and S_4) along with a flying capacitor C_1. The

979-8-3315-1611-6/25/$31.00 ©2025 IEEE

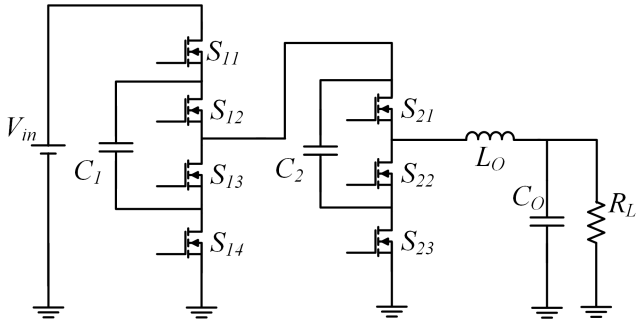

Fig. 1: The 7-Switch ZIV converter introduced in [1]

second stage comprises three switches (M_1, M_2, and M_3) and a flying capacitor C_2. Additionally, the output filter is formed by the inductor L_O and the capacitor C_O. In the diagram, the input source and output load are represented by V_{in} and R_L, respectively.

It is important to note that the original converter is referred to as a ZIV converter, as the voltage across the inductor remains at zero. However, in this control method, the voltage across the inductor is not necessarily zero in the whole voltage conversion range but is maintained at a low level, which minimizes the inductor current ripple. In this context, the term "ZIV" is used to describe the original converter topology.

II. THE PRINCIPLE OF THE NEW CONTROL METHOD

In this section, the basic principle for voltage conversion ratio extension for a seven-switch ZIV converter will be briefly explained. The converter's voltage gain inherently is ¼ as discussed in [1]. Based on the duty cycle value, the operation of the converter is divided into four modes.

A. Mode I: Duty cycle range from 0 to 1/4

The pulse pattern, inductor's current, and the equivalent circuit in a switching cycle for the $0 \leq D \leq 1/4$ are presented in Fig.2. Here the duty cycle (D) is defined as $(t_1 - t_0)/T_s$. In this mode:

1) Switches S_1 and S_3 are activated simultaneously at the start of the switching cycle and remain on for a duration of DT_S before turning off.
2) Switches S_2 and S_4 also turn on together at $t = T_S/4$ and stay on for DT_S before turning off.
3) Switch M_1 turns on at $t = T_S/2$ and stays on for $2DT_S$.
4) Switch M_2 operates in complement to M_1, so when M_1 is off, M_2 is on, and vice versa.
5) Lastly, switch M_3 turns on as S_2 turns off and stays on until the end of the switching cycle.

Fig. 2 also indicates the voltage across the inductor at each switching interval. Accordingly, the inductor current variation in each interval can be calculated as:

$$\Delta i_{Lo11} = (V_{in} - V_{C1} - V_{C2} - V_O)DT_S/L_O \quad (1)$$

$$\Delta i_{Lo12} = (-V_O)(0.25 - DT_S)/L_O \quad (2)$$

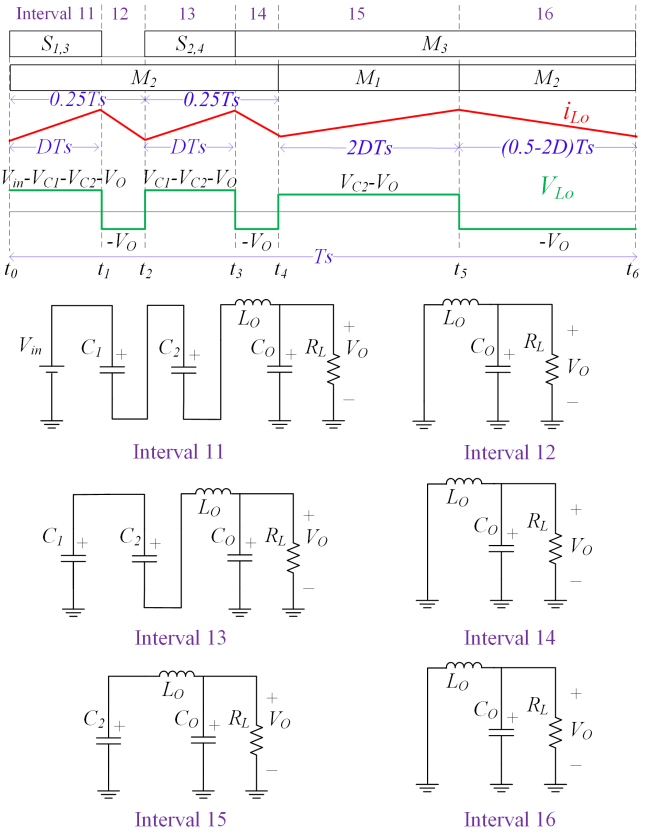

Fig. 2: The pulse pattern, inductor's current and voltage waveforms, and the equivalent circuit of the ZIV converter in each interval in Mode I.

$$\Delta i_{Lo13} = (V_{C1} - V_{C2} - V_O)DT_S/L_O \quad (3)$$

$$\Delta i_{Lo14} = (-V_O)(0.25 - DT_S)/L_O \quad (4)$$

$$\Delta i_{Lo15} = (V_{C2} - V_O)2DT_S/L_O \quad (5)$$

$$\Delta i_{Lo12} = (-V_O)(0.5 - 2DT_S)/L_O \quad (6)$$

where D in the duty cycle, and Δi_{L11}, Δi_{L12}, Δi_{L13}, Δi_{L14}, Δi_{L15}, and Δi_{L16} are inductor's current variations in interval 1 to 6 of $ModeI$, respectively. V_{C1} and V_{C2} are flying capacitors' voltage, and T_S is the switching period.

B. Mode II: Duty cycle range from 1/4 to 1/3

The pulse pattern, inductor's current, and the equivalent circuit in a switching cycle for the $1/4 \leq D \leq 1/3$ are presented in Fig.3. In this mode:

1) Switches S_1 and S_3 turn on simultaneously at the start of the switching cycle and turn off after DT_S.
2) Switches S_2 and S_4 turn on at $t = DT_S$ and turn off at $t = 2DT_S$.
3) Switch M_1 turns on at $t = 2DT_S$ and stays on for a period of $2DT_S$, extending partially into the next switching cycle.

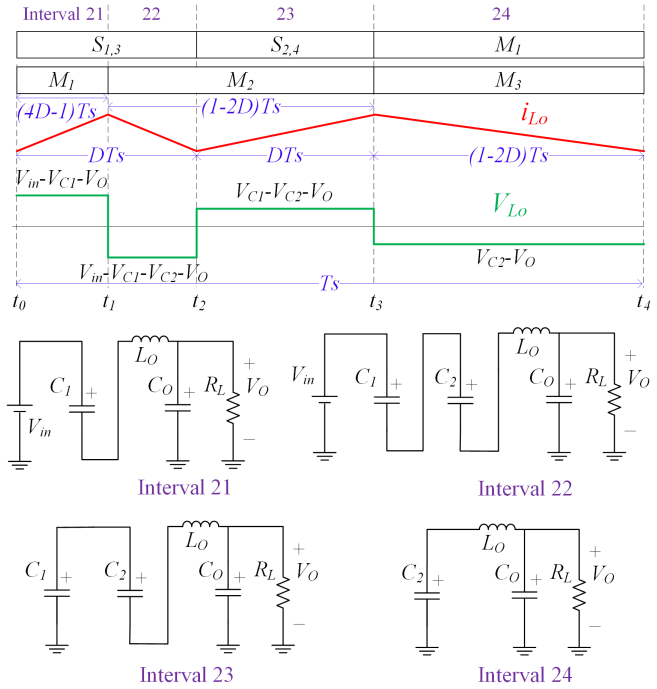

Fig. 3: The pulse pattern, inductor's current and voltage waveforms, and the equivalent circuit of the ZIV converter in each interval in Mode II.

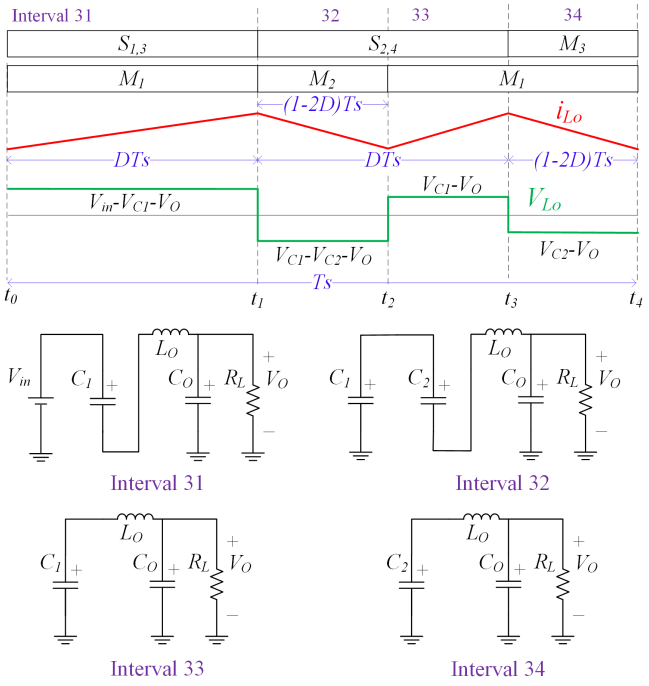

Fig. 4: The pulse pattern, inductor's current and voltage waveforms, and the equivalent circuit of the ZIV converter in each interval in Mode III.

4) Switch M_2 operates in complement to M_1, meaning it turns on whenever M_1 is off and vice versa Consequently, M_2 turns on at $t = (4D-1)T_S$ and turns off at $t = 2DT_S$.
5) Finally, switch M_3 turns on as S_2 and S_4 turn off $t = 2DT_S$ and turns off at the end of the switching cycle.

The voltage across the inductor at each switching interval is also indicated in Fig. 3. Accordingly, the inductor current variation in each interval can be calculated as:

$$\Delta i_{Lo21} = (V_{in} - V_{C1} - V_O)(4D-1)T_S/L_O \quad (7)$$

$$\Delta i_{Lo22} = (V_{in} - V_{C1} - V_{C2} - V_O)(1-3D)T_S/L_O \quad (8)$$

$$\Delta i_{Lo23} = (V_{C1} - V_{C2} - V_O)DT_S/L_O \quad (9)$$

$$\Delta i_{Lo24} = (V_{C2} - V_O)(1-2D)T_S/L_O \quad (10)$$

where Δi_{L21}, Δi_{L22}, Δi_{L23}, and Δi_{L24} are inductor's current variations in interval 1 to 4 of Mode II, respectively.

C. Mode III: Duty cycle range from 1/3 to 1/2

The pulse pattern, inductor's current, and the equivalent circuit in a switching cycle for the $1/3 \leq D \leq 1/2$ are presented in Fig.4. In this mode:

1) Switches S_1 and S_3 turn on together at the beginning of the switching cycle and turn off after DT_S.
2) Switches S_2 and S_4 also turn on at $t = DT_S$ and turn off at $t = 2DT_S$.
3) Switch M_1 turns on at $t = (1-D)T_S$ and stays on for $2DT_S$, completing part of this duration in the next switching cycle. In this mode, M_1 turns off at the same time as S_1 and S_3.
4) Switch M_2 operates in a complementary manner to M_1,
5) Finally, switch M_3 turns on when S_2 and S_4 turn off $(t = DT_S)$ and stays on until the end of the switching cycle.

According to the data presented in Fig. 3, the inductor current variation in each interval can be calculated as:

$$\Delta i_{Lo31} = (V_{in} - V_{C1} - V_O)DT_S/L_O \quad (11)$$

$$\Delta i_{Lo32} = (V_{C1} - V_{C2} - V_O)(1-2D)T_S/L_O \quad (12)$$

$$\Delta i_{Lo33} = (V_{C1} - V_O)(3D-1)T_S/L_O \quad (13)$$

$$\Delta i_{Lo34} = (V_{C2} - V_O)(1-2D)T_S/L_O \quad (14)$$

where Δi_{L31}, Δi_{L32}, Δi_{L33}, and Δi_{L34} are inductor's current variations in interval 1 to 4 of Mode III, respectively.

D. Mode IV: Duty cycle range from 1/1 to 1

The pulse pattern, inductor's current, and the equivalent circuit in a switching cycle for the $1/2 \leq D \leq 1$ are presented in Fig.5. In this mode:

1) Switch S_1 turns on at the start of the switching cycle and turns off after a duration of DTS.

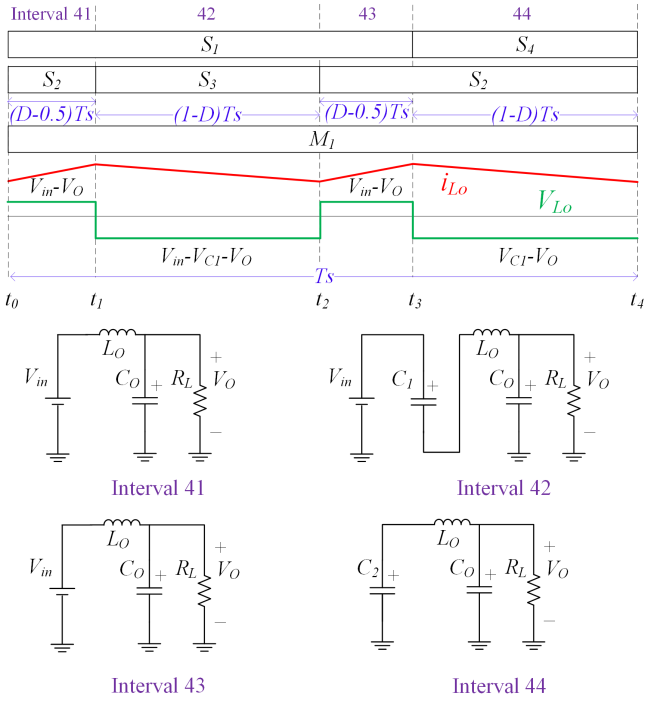

Fig. 5: The pulse pattern, inductor's current and voltage waveforms, and the equivalent circuit of the ZIV converter in each interval in Mode II.

2) Switch S_2 turns on at $t = DT_S/2$ and remains on for DTS, extending partially into the next switching cycle, and turns off at $t = (D - 0.5)T_S$.
3) Switch S_3 operates in complement to S_2.
4) Switch S_4 operates in complement to S_1.
5) Switch M_1 remains continuously on, bypassing the second stage.
6) Switches M_2 and M_3 are always off.

According to the data presented in Fig. 5, the inductor current variation in each interval can be calculated as:

$$\Delta i_{Lo41} = (V_{in} - V_O)(D - 0.5)T_S/L_O \quad (15)$$

$$\Delta i_{Lo42} = (V_{in} - V_{C1} - V_O)(1 - D)T_S/L_O \quad (16)$$

$$\Delta i_{Lo43} = (V_{C1} - V_O)(D - 0.5)T_S/L_O \quad (17)$$

$$\Delta i_{Lo44} = (V_{C1} - V_O)(1 - D)T_S/L_O \quad (18)$$

where Δi_{L41}, Δi_{L42}, Δi_{L43}, and Δi_{L44} are inductor's current variations in interval 1 to 4 of Mode IV, respectively.

III. PERFORMANCE ANALYSIS OF THE CONTROL METHOD

Applying volt-second balance to the inductor at each mode, the voltage gain will be achieved as:

$$V_O = DV_{in} \quad (19)$$

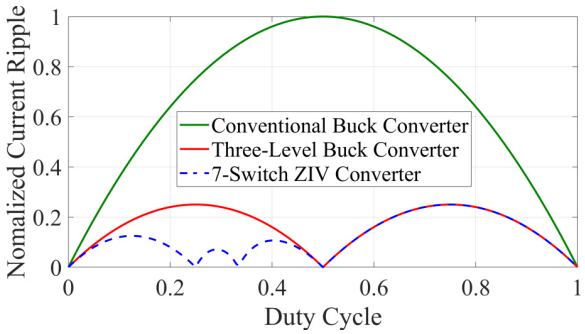

Fig. 6: Current ripple comparison among buck, TLBC, and ZIV converter.

TABLE I: Prototype specifications.

Parameters	Value
V_{in}	$20 - 60V$
V_O	$12V$
I_O	$21A$
P_O	$250W$
F_S	$100kHz$
C_1	$7 \times 10uF/50V$
C_2	$7 \times 10uF/50V$
C_O	$10 \times 10uF/50V$
L_O	$2.2uH$
$S_1 - S_4$	$BSZ025N04LS, 40V/2.5m\Omega$
$M_1 - M_3$	$BSiSA04DN, 30V/2.15m\Omega$

Therefore, the ZIV converter can fully regulate the output voltage from zero to V_{in}, like a Buck converter. However, as mentioned earlier, it is desired to eliminate the buck converter's disadvantages, even having merits over TLBC.

Fig. 6 presents a comparison of the inductor current ripple across the conventional Buck converter, TLBC, and the ZIV converter, with each ripple normalized to the maximum ripple observed in the buck converter. It is evident that both the TLBC and ZIV converters significantly reduce the current ripple compared to the Buck. While the TLBC and ZIV converters show similar current ripple levels for $D > 0.5$, the ZIV converter demonstrates a marked improvement in ripple reduction for $D < 0.5$. This improvement is particularly notable since most operating points typically fall within this range. As a lower current ripple leads to a reduced RMS current, the ZIV converter is expected to be more efficient overall. In addition, a low current ripple enables the use of a smaller inductor, which is highly desirable in recent designs. A smaller inductor significantly increases power density, as magnetic components occupy most of the converter's volume.

IV. EXPERIMENTAL RESULTS AND COMPARISON

The experimental results based on the specifications listed in Table I, are presented in Fig. 7. The gate-pulse for S_1, S_2, and M_1 along with the inductor's current waveform are presented in this figure. The results show the transition conditions that

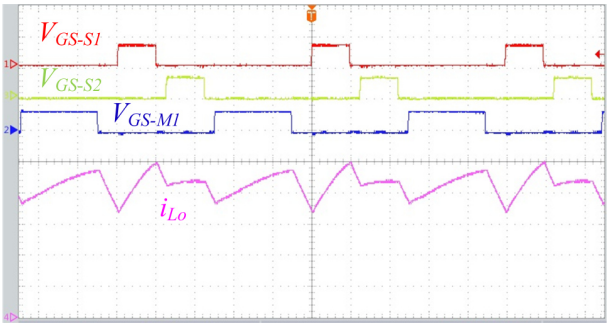

(a) D=0.2 (Mode I)

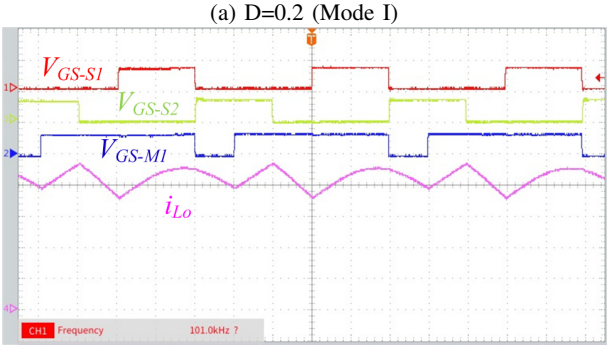

(b) D=0.3 (Mode II)

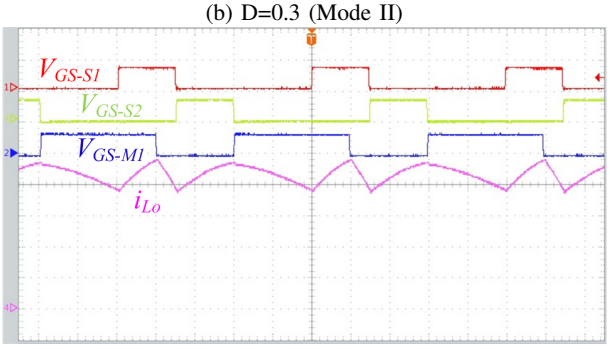

(c) D=0.4 (Mode III)

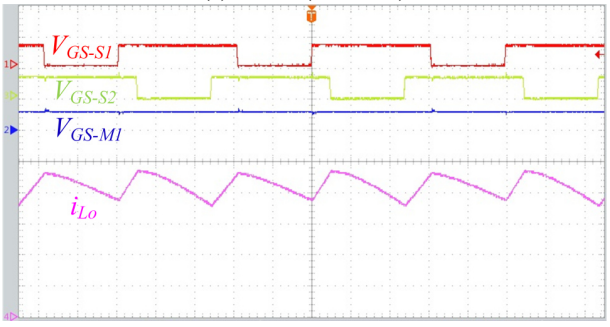

(d) D=0.6 (Mode IV)

Fig. 7: Experimental waveforms for $V_{GS-S1}[5V/div.]$, $V_{GS-S2}[5V/div.]$, $V_{GS-M1}[5V/div.]$, and $i_{Lo}[5A/div.]$, $(t = 2us/div.)$.

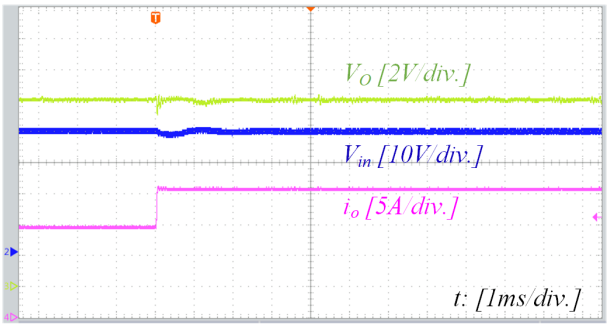

(a)

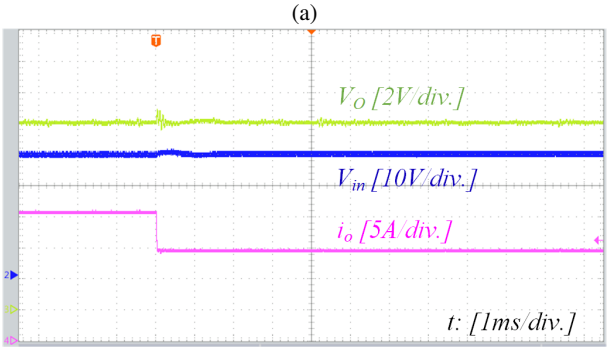

(b)

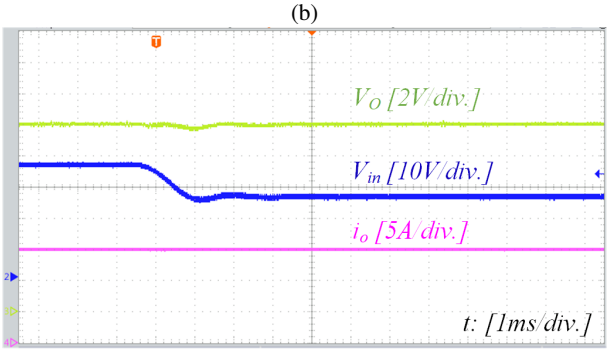

(c)

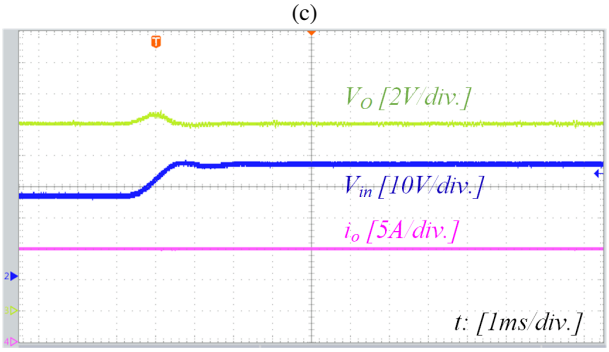

(d)

Fig. 8: Dynamic response of the ZIV converter with the new control method to (a) Load step up, (b) load step down, (c) input voltage step up, and (d) input voltage step down.

cover all four sections that were discussed before. The output current is 21A, and the converter has kept the current ripple low during the transitions.

A controller is designed for the converter to finely tune the output voltage at line and load variations. The converter's dynamic response to these variations is shown in Fig. 8. In particular, Fig. 8(a) illustrates the response to a load increase from 15A to 21A, while Fig. 8(b) depicts the response to a

load decrease from 21A to 15A, both occurring at a slew rate of 0.5A/µs. Throughout these tests, the input voltage remains constant at 40V, and the output voltage is regulated to 12V. The controller successfully stabilizes the output voltage to the new operating point within 200µs in both scenarios.

This rapid response underscores the control system's efficiency in maintaining output stability during sudden load transitions, ensuring minimal voltage deviation and fast recovery, critical for applications requiring high power accuracy and dynamic load handling.

Additionally, Fig. 8(c) and (d) illustrate the converter's dynamic response to line regulation, where the input voltage shifts from 27V to 37V and back, with a slew rate of 10V/ms and a constant load of 15A. The transient time is around 1ms. The converter's ability to quickly respond to line fluctuations ensures reliable operation in environments with unstable power supplies, making it highly adaptable for applications where both load and line stability are vital.

The efficiency of the ZIV converter with the proposed method is compared with two Bucks and a TLBC from EPC [8], [9] in Fig. 9. In Fig 9 (a), the efficiency of the Buck with GaN switches is shown. It is a product from EPC with part number EPC9205. The operation condition is $V_{in} = 48V, V_O = 12V, I_O = 2 - 15A$ (here it is named Buck I). The switching frequency is 700kHz, and the output inductor is 2.2uH. The maximum efficiency of the converter is 95.9%, and at full load, it is 95.3%.

Fig. 9 (b) shows the efficiency comparison between the TLBC and a comparative design of another Buck converter (here it is named Buck II), both from EPC. In this figure, Buck II operates at 500kHz with a 3.3uH inductor. While the TLBC operates at 320kHz, yielding an effective switching frequency of 640kHz, and uses a 1.5uH inductor with 50% less volume than the conventional two-level buck converter. At full load, TLBC achieves a 25% reduction in power loss and over 1% improvement in peak efficiency compared to Buck II, owing to reduced switching stresses and a lower effective switching frequency. The peak and full load efficiency of the TLBC are 96.8% and 96%, respectively.

The efficiency of the ZIV converter is compared with TLBC, Buck I, and Buck II in Fig. 9(c), under the same condition. The ZIV converter has significantly improved efficiency over the whole output power range from 3A to 21A. This is because the conversion ratio is ¼ which is one of the ZIV points. According to Fig. 6, at this point, the current ripple of the ZIV converter is zero, while in a TLBC and a Buck, it is 25% and 60% of the maximum current ripple in a Buck converter, respectively. In Fig. 9(b), it was mentioned that the reason for the efficiency improvement of TLBC over Buck II is the lower current ripple. Consequently, in the ZIV converter, since the current ripple is minimized, the efficiency is higher than TLBC.

The peak and full load efficiency of the four converters is listed in Table II, as well as the average efficiency over the whole output current range. The range of current over which the average efficiency is calculated is indicated in the

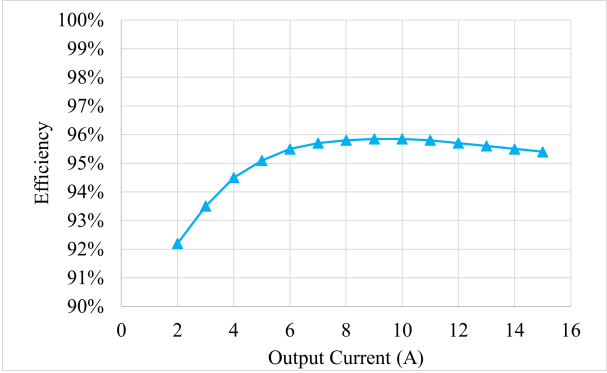

(a) Efficiency curve of Buck I [9],

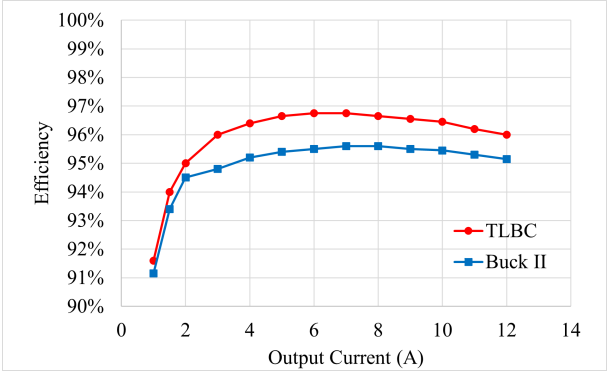

(b) Efficiency curve of TLBC [8] and Buck II [8],

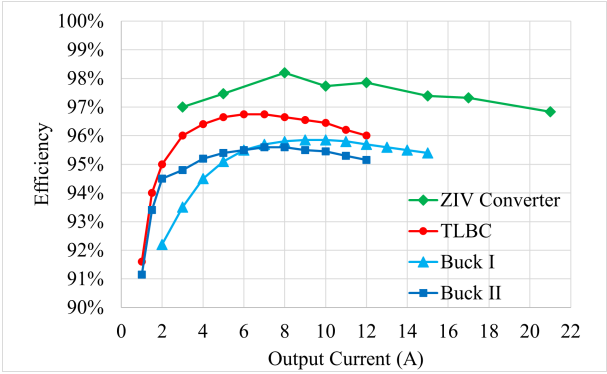

(c) Efficiency comparison of the ZIV converter, Buck I [9], Buck II [8], and TLBC [8].

Fig. 9: Efficiency curves of the converters

corresponding row. The peak and full load efficiency of the ZIV converter (even at 21A) is more than the other ones. Although the output current range of the ZIV converter is more than the others, its average efficiency is 1.9% more than Buck I, 2.2% more than Buck II, and 1.2% more than TLBC. The efficiency of the ZIV converter from light load to full load, including the control and drivers' loss is shown in Fig. 10. The average efficiency at light load is 97.7%, and at full load, it is 97.12%. The peak efficiency is 98.5% which occurs at light load. Also, the average efficiency over the whole input voltage and power range is 97.54%. Moreover, the efficiency curve is almost flat during the input voltage range and at

TABLE II: EFFICIENCY COMPARISON OF THE CONVERTERS

	Peak Efficiency	Full Load Efficiency	Average Efficiency
Buck I [9]	95.9%	95.4% @15A	95.6% [5A-15A]
Buck II [8]	95.6%	95.2% @12A	95.3% [2A-12A]
TLBC [8]	96.8%	96% @12A	96.3% [2A-12A]
This work	**98.2%**	**97.4% @15A 96.8% @21A**	**97.5% [3A-21A]**

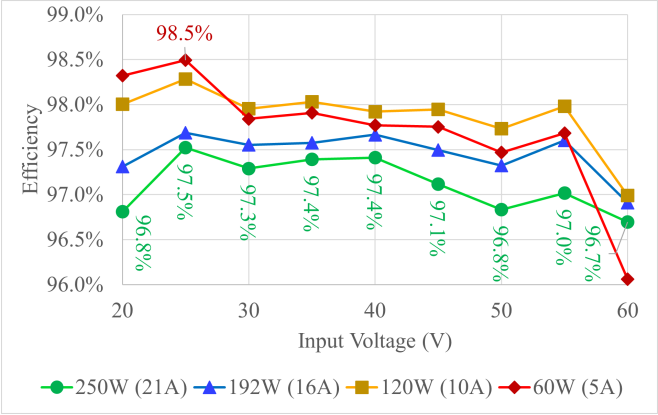

Fig. 10: The measured efficiency of the ZIV converter versus input voltage at various output power.

different output power levels. This shows that the converter preserves high and almost constant efficiency throughout the input voltage and power.

V. THE CONVERTER'S PERFORMANCE IN A SOLAR BATTERY CHARGER APPLICATION

This converter was used in a solar battery charger application, and the corresponding experimental results will be discussed in this section to validate the feasibility of the new control method further.

In this application, TerraSAS ETS 600/17 was used as a solar simulator. Also, an LC input filter ($C_f = 100uF, L_f = 8uH$) was used to make the input current smooth. To examine the functionality of the proposed control method in a dynamic environment, the irradiation of the solar emulator was set to change in 30-second intervals from $100W/m^2$ to $1000W/m^2$, as shown in Fig. 10. In this condition, the input voltage changes from 28.5V to 45V. The output voltage is fixed at 12V, by a constant voltage load (to mimic a battery), and the maximum power is 180W. The converter is set to do the Maximum Power Point Tracking (MPPT) with the Perturb and Observation (P&O) method. Fig. 11 shows the experimental results for the MPPT performance of the converter with the new control method. The maximum available power and the harvested power are presented in this figure. The irradiation changes every 30 seconds with a one-second transition between the levels. The irradiation changing pattern is repeated twice for the dynamic performance investigation, and then it is kept constant to explore the static functionality. At each irradiation level, its value is indicated in this figure. The MPPT efficiency, defined as the ratio of the harvested power to the maximum available power, is illustrated in Fig. 11 for various irradiation levels. The efficiency is mostly more than 99%. This figure demonstrates that the control method effectively tracks the maximum power point under both increasing and decreasing irradiation conditions, ensuring optimal power extraction. As shown, the converter successfully adapts to changes in irradiation, maintaining high MPPT efficiency and maximizing the harvested power across a range of environmental conditions. This adaptability is essential for efficient energy capture in applications where sunlight varies frequently. Consequently, as discussed in Section IV, The converter can effectively adapt to rapid dynamic changes.

VI. CONCLUSION

This paper investigates a novel control method for the 7-switch ZIV converter that maximizes its voltage conversion range without requiring additional components or feedback signals. The converter's voltage conversion range is divided into four sections, with smooth transitions between them, ensuring that there is no sudden shift in the phase or duty cycle of any switch. The ZIV converter has the same voltage conversion ratio as a traditional buck converter but offers a significantly reduced inductor current ripple, which contributes to higher efficiency. The comparative study showed that the efficiency of the ZIV converter is higher than that of a TLBC built with GaN technology and fewer switches. The converter's dynamic response was evaluated under both line and load regulation conditions, with results indicating excellent stability and adaptability to changes. Additionally, the converter was tested in a solar battery application, where it was configured to maintain a constant load voltage while tracking maximum power at the input. Under these conditions, the MPPT efficiency proved to be outstanding, validating the controller's effectiveness in applications with variable input conditions like solar energy harvesting.

REFERENCES

[1] S. Webb, T. Liu and Y. -F. Liu, "Zero Inductor-Voltage Multilevel Bus Converter," in IEEE Transactions on Power Electronics, vol. 36, no. 10, pp. 11565-11578, Oct. 2021.

[2] M. Uno and A. Kukita, "PWM Switched Capacitor Converter With Switched-Capacitor-Inductor Cell for Adjustable High Step-Down Voltage Conversion," in IEEE Transactions on Power Electronics, vol. 34, no. 1, pp. 425-437, Jan. 2019.

[3] S. Han, Y. Wang, Y. Guan and D. Xu, "Analysis and Design of a Modular Switched Capacitor Converter with Adjustable Output Voltage in DC Microgrid," in IEEE Journal on Emerging and Selected Topics in Circuits and Systems, vol. 12, no. 1, pp. 232-241, March 2022.

[4] H. Setiadi and H. Fujita, "An Asymmetric Control Method for Switched-Capacitor-Based Resonant Converters," in IEEE Transactions on Power Electronics, vol. 36, no. 9, pp. 10729-10741, Sept. 2021.

[5] Y. Li, B. Curuvija, X. Lyu and D. Cao, "Multilevel modular switched-capacitor resonant converter with voltage regulation," 2017 IEEE Applied Power Electronics Conference and Exposition (APEC), Tampa, FL, USA, 2017, pp. 88-93.

[6] G. Ripamonti, M. Ursino, S. Saggini, S. Michelis and F. Faccio, "Regulated Resonant Switched-Capacitor Point-of-Load Converter Architecture and Modeling," in IEEE Transactions on Power Electronics, vol. 36, no. 4, pp. 4815-4827, April 2021.

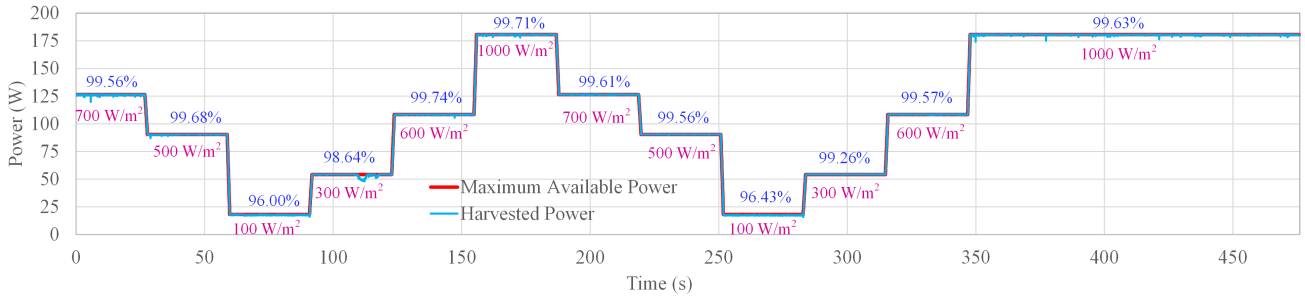

Fig. 11: The experimental results for MPPT performance of the ZIV converter with the new control method in dynamic and static conditions.

[7] A. Cervera, M. Evzelman, M. M. Peretz and S. Ben-Yaakov, "A High-Efficiency Resonant Switched Capacitor Converter with Continuous Conversion Ratio," in IEEE Transactions on Power Electronics, vol. 30, no. 3, pp. 1373-1382, March 2015.

[8] D. Reusch, S. Biswas and M. de Rooij, "GaN Based Multilevel Intermediate Bus Converter for 48 V Server Applications," PCIM Europe 2018; International Exhibition and Conference for Power Electronics, Intelligent Motion, Renewable Energy and Energy Management, Nuremberg, Germany, 2018, pp. 1-8.

[9] Efficient Power Conversion, " Development Board EPC9205 Quick Start Guide," EPC9502 Datasheet, 2018.